Practically stable unstable orthorhombic finite differences

Huy Le and Stewart A. Levin

ABSTRACT

Intrigued by an instability result presented at the last SEG meeting (Chu, 2012), we analyze it and some variants to understand the nature and extent of such instabilities. We investigate an unexpected dependency of stability on the order of our spatial derivative approximation. We find that even the apparently stable scheme in that SEG abstract is actually slightly unstable, though the instability is not qualitatively manifest until tens of thousands of time steps are taken.

INTRODUCTION

The Stanford Exploration Project, in line with the interests of many of its sponsors, has been investigating the effects of anisotropy on seismic processing, imaging and inversion. Much recent interest in the geophysical community has focused on the effects of orthorhombic symmetry, a type of elastic symmetry that has three mutually orthogonal planes of symmetry. This type of symmetry can be found, most commonly, where a set of vertical fractures is embeded in a VTI medium, or where two identical sets of fractures make an arbitrary angle to each other, or where two or three sets of mutually perpendicular fractures intersect (Tsvankin, 1997). Orthorhombic crystals occur in anhydrite, olivine, and sulfur.

An orthorhombic medium is characterized by nine independent elastic parameters, c_{ij}, that enter into a linear Christoffel relationship between stresses, σ_{ij}, and strains, ϵ_{ij} (Malvern, 1969):

$$\begin{bmatrix} \sigma_{11} \\ \sigma_{22} \\ \sigma_{33} \\ \sigma_{23} \\ \sigma_{31} \\ \sigma_{12} \end{bmatrix} = \begin{bmatrix} c_{11} & c_{12} & c_{13} & & & \\ c_{12} & c_{22} & c_{23} & & & \\ c_{13} & c_{23} & c_{33} & & & \\ & & & c_{44} & & \\ & & & & c_{55} & \\ & & & & & c_{66} \end{bmatrix} \begin{bmatrix} \epsilon_{11} \\ \epsilon_{22} \\ \epsilon_{33} \\ 2\epsilon_{23} \\ 2\epsilon_{31} \\ 2\epsilon_{12} \end{bmatrix}. \tag{1}$$

There are two common ways to derive equations for wave propagation in anisotropic media. The first approach is to derive them from the dispersion relations obtained from the general Christoffel equations (Alkhalifah, 2003). The resultant differential equations are sixth-order in both time and space. Another approach is to start with

constitutive stress-strain relations and equations of motion (Duveneck and Bakker, 2011; Zhang and Zhang, 2011). The resultant equations from this approach are second order. In either case, these are systems that couple both normal and shear stresses.

In practice, we are currently most interested in analysis and imaging of compressional waves. For this case, one approximation is to set the shear velocities in the symmetry plane axes to zero ($c_{44} = c_{55} = c_{66} = 0$), resulting in what are called *pseudo-acoustic* wave equations. This substitution reduces the medium description to six parameters instead of nine. Following the second approach, in tilted orthorhombic symmetry, the system of pseudo-acoustic wave equations takes the following form:

$$\frac{\partial^2 \sigma_{ii}}{\partial t^2} = \sum_j G_{ij} \sum_m \sum_n R_{jm} R_{jn} \sum_l \frac{\partial^2}{\partial x_n \partial x_l} \sum_k R_{km} R_{kl} \sigma_{kk}, \tag{2}$$

where σ_{ii} are three normal stresses, G_{ij} are related to vertical P-wave velocity v_{pz} and the Thomsen anisotropic parameters ϵ_i and δ_i in symmetry planes, and the R_{ij} are entries of the matrix that transforms from the coordinate system aligned with the symmetry of the material to the surface North-East South-West Vertical system (Chu, 2012).

We reparameterize system 2 as:

$$\frac{\partial^2 \sigma_{ii}}{\partial t^2} = \sum_{n,l,k} a_{inlk} \frac{\partial^2}{\partial x_n \partial x_l} \sigma_{kk}, \tag{3}$$

where

$$a_{inlk} = \sum_{j,m} G_{ij} R_{jm} R_{jn} R_{km} R_{kl} \tag{4}$$

are the corresponding coefficients in front of the spatial derivatives. These a_{inlk} coefficients have units of velocity squared. This reparameterization simplifies later algebraic manipulations and analysis and reduces the computational time significantly.

Relation 3 defines a system of three second-order coupled equations for the three normal stresses σ_{ii}. The compressional pressure P-wave is defined as the negative of the average of these stresses, $p = -\frac{1}{3}\sum_i \sigma_{ii}$ (Malvern, 1969). Each of the equations in 3 has 18 terms on the right-hand side: nine non-mixed spatial derivatives and nine mixed spatial derivatives. The mixed derivatives consume a major fraction of the computational time as compared to the non-mixed ones and will be handled differently by different numerical schemes.

NUMERICAL STABILITY ANALYSIS

We analyze the stability of three different numerical schemes, following Chu (2012). All of them use centered finite differences to approximate the non-mixed second spatial derivatives. They differ in how the mixed derivatives are calculated (Table 1).

	Non-mixed derivatives	Mixed derivatives
Scheme 1	Centered	Centered
Scheme 2	Centered	Rotated non-staggered
Scheme 3	Centered	Rotated staggered

Table 1: Numerical schemes we analyze for stability.

To analyze the stability of system 3, we use the von Neumann method (Saenger et al., 2000; Richtmyer and Morton, 1957). Rewriting system 3 in matrix form we have

$$\frac{\partial^2 \boldsymbol{\sigma}}{\partial t^2} = \mathbf{L}\boldsymbol{\sigma}, \tag{5}$$

where $\boldsymbol{\sigma} = [\sigma_{ii}]$ is a vector of three normal stresses, and $\mathbf{L}$ is a 3×3 matrix differential operator.

The numerical approximation of equation 5 in the spatial Fourier domain takes the following form:

$$\hat{\boldsymbol{\sigma}}_{n+1} = (\triangle t^2 \hat{\mathbf{L}} + 2\mathbf{I})\hat{\boldsymbol{\sigma}}_n - \hat{\boldsymbol{\sigma}}_{n-1}, \tag{6}$$

where we have used second-order finite difference in time with step size $\triangle t$. The hat notation represents a function in the spatial Fourier domain, and the subscript denotes time level.

Equation 6 is a three-level recursive relation between the future ($t = n+1$), current ($t = n$), and past ($t = n-1$) wavefields. It can be reduced to a two-level system of equations as follows:

$$\begin{bmatrix} \hat{\boldsymbol{\sigma}}_{n+1} \\ \hat{\boldsymbol{\sigma}}_n \end{bmatrix} = \begin{bmatrix} \triangle t^2 \hat{\mathbf{L}} + 2\mathbf{I} & -\mathbf{I} \\ \mathbf{I} & \mathbf{0} \end{bmatrix} \begin{bmatrix} \hat{\boldsymbol{\sigma}}_n \\ \hat{\boldsymbol{\sigma}}_{n-1} \end{bmatrix}, \tag{7}$$

or

$$\mathbf{u}_{n+1} = \mathbf{A}\mathbf{u}_n, \tag{8}$$

where

$$\mathbf{u}_n = \begin{bmatrix} \hat{\boldsymbol{\sigma}}_n \\ \hat{\boldsymbol{\sigma}}_{n-1} \end{bmatrix} \tag{9}$$

is a six-component vector of three current and three previous wavefields and

$$\mathbf{A} = \begin{bmatrix} \triangle t^2 \hat{\mathbf{L}} + 2\mathbf{I} & -\mathbf{I} \\ \mathbf{I} & \mathbf{0} \end{bmatrix} \tag{10}$$

is the 6×6 *amplification* matrix.

The amplification matrix is a function of wave numbers k_x, k_y and k_z and determines how much each mode (in spatial frequency) is amplified as one time step advances. It depends on the medium parameters a_{inlk} (equation 4), the numerical scheme, the order of spatial approximation $M/2$, and the time and space step sizes

(Appendix A). The numerical scheme is stable when the magnitude of the largest eigenvalue of **A** is less than unity for all modes.

In the case of second-order spatial approximation, an exact formula for the eigenvalues of **A** might be found (Saenger et al., 2000). In our case, as shown in Appendix B, finding the explicit form for the eigenvalues of **A** involves solving a cubic equation. In our work, we numerically compute the eigenvalues for different symmetries (Table 2) and analyze how the eigenvalues of **A** vary with changing time step and order of spatial approximation. We choose $\triangle x = \triangle y = 12.5$ m and $\triangle z = 6.25$ m.

Symemtry	ϵ_1	ϵ_2	δ_1	δ_2	δ_3	v_{pz} (m/s)	θ	φ	ϕ
Isotropic	0	0	0	0	0	2000	0	0	0
TI	0.16	0.16	0.06	0.06	0	2000	0	0	0
Orthorhombic	0.2	0.12	0.07	0.05	0	2000	0	0	0
Tilted Orthorhombic	0.2	0.12	0.07	0.05	0	2000	40	25	35

Table 2: Medium parameters we use for stability analysis (Chu, 2012).

RESULTS AND DISCUSSION

For tilted orthorhombic media, from Figures 1(a), 2(a), and 3(a), we observe that the magnitude of the largest eigenvalue increases exponentially with increasing time step $\triangle t$ and, as expected, approaches unity as $\triangle t$ approaches zero. Additionally, higher orders of spatial approximation generally come with higher degrees of instability. This implies a trade-off between accuracy and stability. The largest eigenvalues for schemes 1 and 3 have the same order of magnitude, while those of scheme 2 are considerably greater (Figures 1(b), 2(b), and 3(b)). This illustrates that, as Chu points out, using rotated non-staggered finite differences for approximating mixed spatial second derivatives causes a more severe problem of instability. Although centered and rotated staggered grids have a less serious instability issue, higher order spatial approximations (orders 8th, 10th, 12th, 14th, and 16th) are not technically stable, because their corresponding maximum eigenvalues are slightly greater than unity (Figures 2(b), and 3(b)). However, for typical time steps of a millisecond or less, amplification of the wavefield will not be significant until after tens of thousands of time steps.

Figures 4 and 5 show that the issue of instability becomes much more problematic for tilted orthorhombic media than for other types of symmetries. Also, from these figures, with our particular sets of material parameters, these numerical schemes applied to TI symmetry surprisingly appear to become unstable more quickly than those applied to vertical orthorhombic symmetry. We do not believe this is actually the case, but an artifact of numerical precision when eigenvalues are clustered, as they most certainly are for TI media which has a plane of symmetry. This still needs to be investigated.

One interpretation of the CFL stability condition is that the wavefield should not propagate past multiple grid points in one time step. Consequently, one would intuitively expect that the fast-progagating waves are more likely to cause instability. Our observation that the directions that have the largest eigenvalues do not coincide with the directions of the fast-propagating waves (Figure 6), however, does not fully support this intuition.

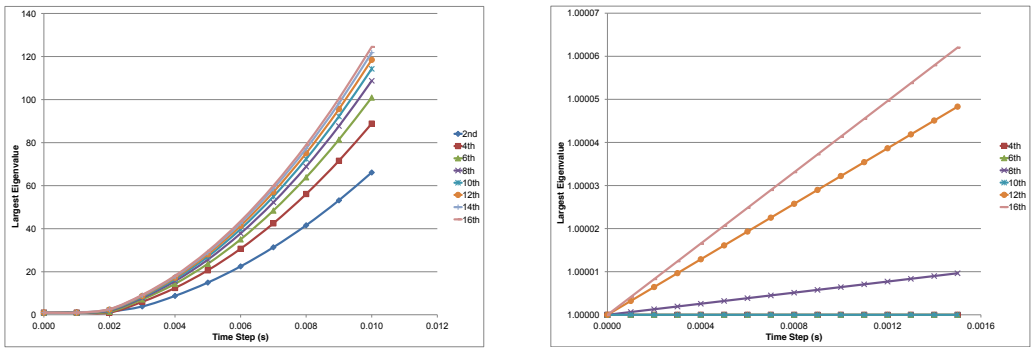

(a) (b)

Figure 1: Largest eigenvalues of different orders for tilted orthorhombic media using scheme 1: (a) large time steps and (b) small time steps. [**NR**]

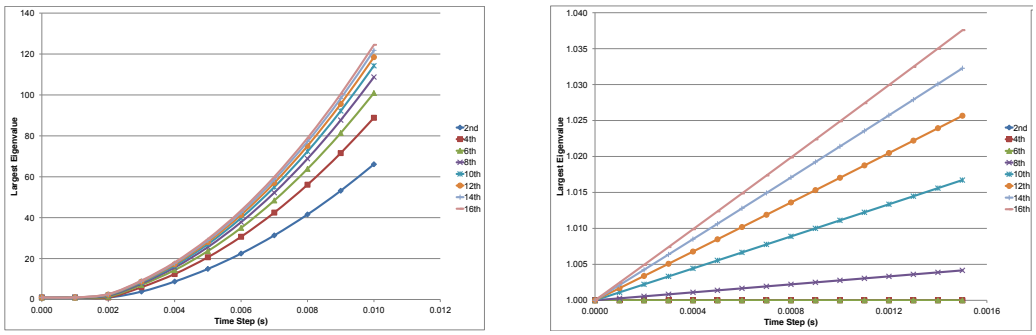

(a) (b)

Figure 2: Largest eigenvalues of different orders for tilted orthorhombic media using scheme 2: (a) large time steps and (b) small time steps. With such eigenvalues, the wavefield would be amplified greatly after hundreds of time steps. [**NR**]

CONCLUSION

We verified that using rotated non-staggered finite difference to approximate the mixed derivatives in wave equations for tilted orthorhombic media can cause serious instability. Alternative schemes, such as centered and rotated staggered finite differences are practically stable, that is, with time steps around or less than a millisecond, the wavefield can be propagated up to tens of thousands of steps without being excessively amplified.

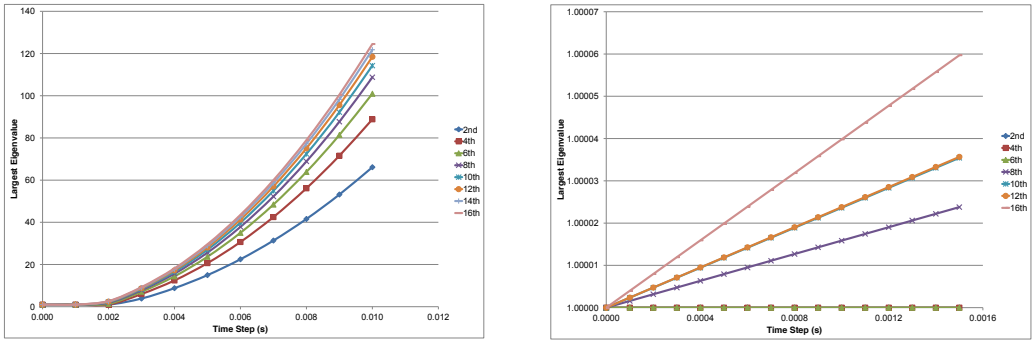

(a) (b)

Figure 3: Largest eigenvalues of different orders for tilted orthorhombic media using scheme 3: (a) large time steps and (b) small time steps. [**NR**]

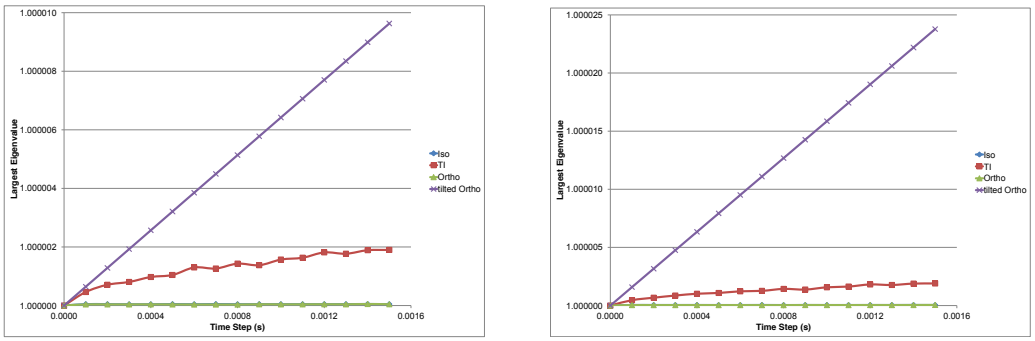

(a) (b)

Figure 4: Largest eigenvalues of 8th order for tilted orthorhombic media using: (a) scheme 1 and (b) scheme 3. [**NR**]

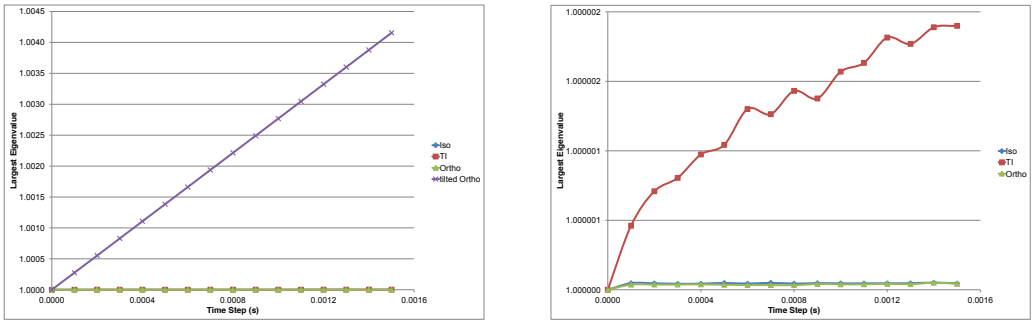

(a) (b)

Figure 5: Largest eigenvalues of 8th order for tilted orthorhombic media using scheme 2: (a) 4 types of symmetries and (b) zoom-in without tilted orthorhombic. [**NR**]

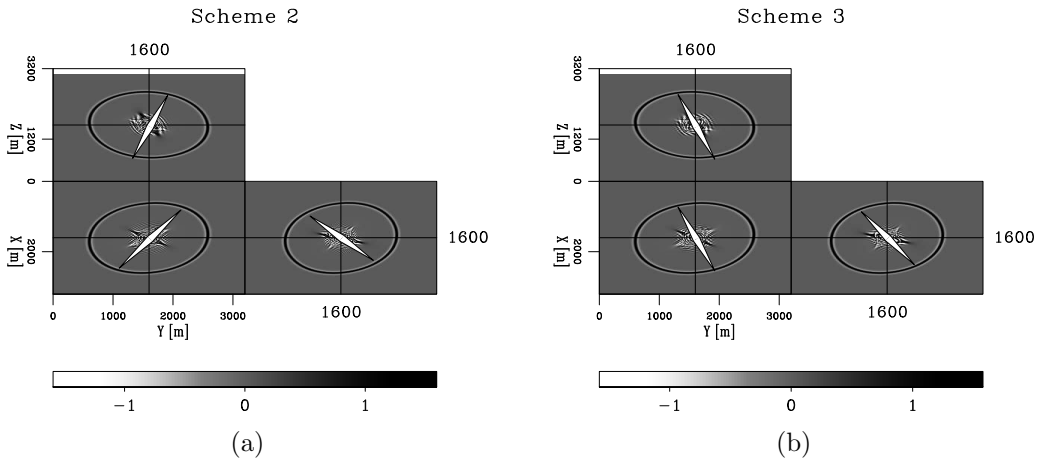

Figure 6: Wavefield snapshots at $t = 0.5$ s using $\triangle t = 0.1$ ms: (a) scheme 2 and (b) scheme 3. The arrows mark directions that have the largest eigenvalues. These directions do not coincide with the directions of the fast-propagating waves. [**CR**]

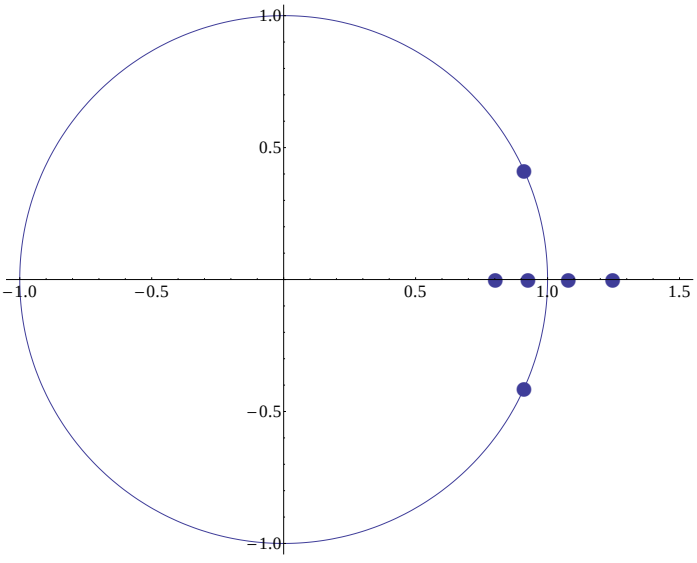

Figure 7: Positions of six eigenvalues of the amplification matrix **A** (for scheme 1, second order spatial approximation, tilted orthorhombic symmetry) with respect to the unit circle. The figure shows three pairs of eigenvalues: one complex-conjugate pair of magnitude unity and two real pairs, each of which has one eigenvalue that is greater than unity. [**NR**]

ACKNOWLEDGMENTS

I would like to thank colleagues and professors at the Stanford Exploration Project for many of their valuable advices and discussions.

APPENDIX A

The amplification matrices are as follows:

For scheme 1:

$$\begin{aligned}\hat{L}_{ik} &= \sum_n a_{innk}\frac{2}{\triangle x_n^2}\sum_{p=1}^{M/2} c_p[cos(k_{x_n}p\triangle x_n)-1] \\ -\sum_{n\neq l}(a_{inlk}+a_{ilnk})&\frac{4}{\triangle x_n\triangle x_l}\sum_{p=1}^{M/2} b_p sin(k_{x_n}p\triangle x_n)\sum_{p=1}^{M/2} b_p sin(k_{x_l}p\triangle x_l).\end{aligned} \tag{A-1}$$

For scheme 2:

$$\begin{aligned}\hat{L}_{ik} &= \sum_n a_{innk}\frac{2}{\triangle x_n^2}\sum_{p=1}^{M/2} c_p[cos(k_{x_n}p\triangle x_n)-1] \\ -\sum_{n\neq l}(a_{inlk}+a_{ilnk})&\frac{1}{\triangle x_n\triangle x_l}\sum_{p=1}^{M/2} c_p sin(k_{x_n}p\triangle x_n)sin(k_{x_l}p\triangle x_l).\end{aligned} \tag{A-2}$$

For scheme 3:

$$\begin{aligned}\hat{L}_{ik} &= \sum_n a_{innk}\frac{2}{\triangle x_n^2}\sum_{p=1}^{M/2} c_p[cos(k_{x_n}p\triangle x_n)-1] \\ -\sum_{n\neq l\neq r}(a_{inlk}+a_{ilnk})&\frac{4}{\triangle x_n\triangle x_l}\sum_{p=1}^{M/2} s_p sin(k_{x_n}\frac{2p-1}{2}\triangle x_n)cos(k_{x_l}\frac{2p-1}{2}\triangle x_l)cos(k_{x_r}\frac{2p-1}{2}\triangle x_r) \\ &\times\sum_{p=1}^{M/2} s_p cos(k_{x_n}\frac{2p-1}{2}\triangle x_n)sin(k_{x_l}\frac{2p-1}{2}\triangle x_l)cos(k_{x_r}\frac{2p-1}{2}\triangle x_r).\end{aligned} \tag{A-3}$$

The c_p, b_p, and s_p are coefficients of the spatial derivative approximations as defined by Chu(2012).

APPENDIX B

Stability is assessed by examing the roots of the determinant of the eigenvalue matrix:

$$\mathbf{A} - \lambda\mathbf{I} = \begin{bmatrix} \triangle t^2\hat{\mathbf{L}} + 2\mathbf{I} - \lambda\mathbf{I} & -\mathbf{I} \\ \mathbf{I} & -\lambda\mathbf{I} \end{bmatrix} \tag{B-1}$$

Due to the commutativity of the identity matrix with all other matrices, the determinant of this block matrix is the same as the determinant of

$$(\triangle t^2\hat{\mathbf{L}} + 2\mathbf{I} - \lambda\mathbf{I}) \cdot (-\lambda\mathbf{I}) - \mathbf{I} \cdot (-\mathbf{I}). \tag{B-2}$$

Simplifying, this becomes

$$\det A = \det((\lambda^2+1)I - \lambda(\triangle t^2\hat{\mathbf{L}} + 2\mathbf{I})) = (-\lambda)^3 \det((\triangle t^2\hat{\mathbf{L}} + 2\mathbf{I}) - (\lambda + 1/\lambda)I). \tag{B-3}$$

This takes the form of the eigenvalue calculation for $\triangle t^2\hat{\mathbf{L}} + 2\mathbf{I}$, with each eigenvalue $\hat{\lambda}$ providing a pair of eigenvalues of $\mathbf{A}$ according to $\hat{\lambda} = \lambda + \frac{1}{\lambda}$. Solving by the quadratic formula yields

$$\lambda = \frac{\hat{\lambda} \pm \sqrt{\hat{\lambda}^2 - 4}}{2}. \tag{B-4}$$

If we assume $\hat{\lambda}$ is real valued, then we first consider the case $|\hat{\lambda}| > 2$. In this event the two roots are real and their product is 1; hence at least one is greater than 1 in magnitude. This situation is therefore unstable. If the magnitude is exactly 2, the roots are either both 1 or both -1, a stable situation. Finally, with the magnitude less than 2, the roots are complex and the squared magnitude of each is

$$|\lambda|^2 = \frac{\hat{\lambda}^2 - (\hat{\lambda}^2 - 4)}{4} = 1; \tag{B-5}$$

in other words, both roots are on the unit circle. These are, indeed, the very situations we observed in our analysis (Figure 7).

REFERENCES

Alkhalifah, T., 2003, An acoustic wave equation for orthorhombic anisotropy: Geophysics, **68**, 1169–1172.

Chu, C., 2012, A hybrid finite difference method for acoustic wave propagation in tilted orthorhombic media: 82nd SEG Ann. Internat. Meeting, Expanded Abstracts, 1–5, Soc. of Expl. Geophys.

Duveneck, E. and P. M. Bakker, 2011, Stable P-wave modeling for reverse-time migration in tilted TI media: Geophysics, **76**, S65–S75.

Malvern, L. E., 1969, Introduction to the mechanics of a continuous medium: Prentice-Hall.

Richtmyer, R. D. and K. W. Morton, 1957, Difference methods for initial-value problems: Interscience Publishers.

Saenger, E. H., N. Gold, and S. A. Shapiro, 2000, Modeling the propagation of elastic waves using a modified finite-difference grid: Wave Motion, **31**, 77–92.

Tsvankin, I., 1997, Anisotropic parameters and P-wave velocity for orthorhombic media: Geophysics, **62**, 1292–1309.

Zhang, H. J. and Y. Zhang, 2011, Reverse-time migration in vertical and tilted orthorhombic media: 81st SEG Ann. Internat. Meeting, Expanded Abstracts, 185–189, Soc. of Expl. Geophys.